

# On Using Ray-Launching Method for Modeling Rotational Spectrometer

Jaroslav LÁČÍK, Zbyněk LUKEŠ, Zbyněk RAIDA

Dept. of Radio Electronics, Brno University of Technology, Purkyňova 118, 612 00 Brno, Czech Republic

lacik@feec.vutbr.cz, lukes@feec.vutbr.cz, raida@feec.vutbr.cz

**Abstract.** In this paper the ray-launching method is developed and used for the modeling of a rotational spectrometer. Since the electrical size of the spectrometer is several thousands times longer compared to the wavelength, the presented approach is much suitable for the analysis of such huge devices than the classical numerical exact methods such as the fast integral methods.

The accuracy of the developed approach is verified on an analysis of a spectrometer component – a lens. Firstly, the lens is analyzed in CST Microwave Studio, and secondly, by the developed ray-launching method. Comparisons show that the accuracy of the developed approach is good.

## Keywords

Ray tracing, ray launching, rotational spectrometer, rotational spectroscopy.

## 1. Introduction

The rotational spectroscopy investigates the absorption and the emission of electromagnetic radiation in the microwave frequency range. The absorption and the emission are caused by molecules, and correspond to the change of the rotational quantum number of molecules. The rotational spectroscopy can be practically used for the substance in the gas phase only where the rotational motion of molecules is quantized. The corresponding frequencies of the absorption range from tens to hundreds of gigahertz.

The block scheme of the rotational spectrometer is depicted in Fig. 1 [1]. A synthesizer whose frequency is controlled by a rubidium standard generates a microwave signal. The signal is amplified, multiplied (in order to reach a desired frequency), transmitted by an antenna and focused by a lens. A linearly polarized wave propagates through a polarization filter to a sample cell. The sample cell, which length is in the order of decimeters or meters, is filled by an analyzed gas of low pressure. After passing the sample cell, the wave is reflected back by a roof mirror, which changes the wave polarization. The reflected wave is deflected by the polarization grid and received by a receive antenna. Then, the received signal is detected and processed by a computer. Thus, the rotational (absorption) line

spectrum of an analyzed gas is obtained.

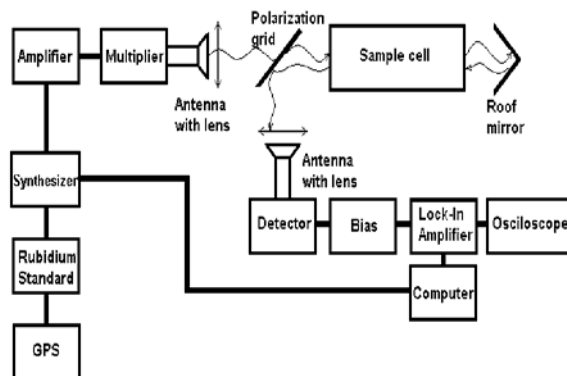


Fig. 1. Block diagram of a rotational spectrometer.

Typical electrical size of the rotational spectrometer is in order of thousands of wavelength. Evidently, it is an electrically large object, and therefore, conventional numerical methods can not be used for its analysis due to their insufficient efficiency. And that is the reason for applying geometrical optics, and ray tracing methods for its analysis.

There are direct and indirect methods of ray tracing. Direct methods, e.g. image theory, are based on finding all the relevant propagation paths from a source point to a desired observation point. In case of indirect methods (so called “ray launching”), a number of rays is launched from a source point in arbitrary directions, and traced to hit the receiver or reach a certain maximum attenuation. In order to ensure that all the relevant propagation paths are found, a large number of rays have to be transmitted. However, the decision whether a ray hits a receiver or not is difficult. There are two decision methods: the discrete ray tubes [3] or the reception spheres [4], and the discrete rays. Since the method of the discrete ray tubes does not work properly at curved boundaries, the modification of the reception spheres is used for the analysis of the spectrometer.

When using the method of the reception spheres, the determination of the diameter of spheres is difficult because important propagation paths may not be considered (the diameter is too large), or several physically identical rays reach the receiver (the diameter is too small). In order to overcome this trouble, the ray density normalization (RDN) can be applied. Moreover, the original approach [5] does not take into account diffracted fields.

The paper is organized as follows. Section 2 summarizes basic principles of the geometrical optics and the uniform theory of diffraction used for the ray-tracing methods. In section 3, the ray density normalization is extended in order to take diffracted fields into account. In addition, the power-field approach is proposed for the evaluation of the field of launched rays. Section 4 is focused on the verification of the developed ray launching approach, and on modeling the rotational spectrometer. Finally, Section 5 concludes the paper.

## 2. Geometrical Optics

Geometrical optics (GO) is an approximate high-frequency method for determining wave propagation for incident, reflected and refracted fields. Since GO uses ray concepts, GO is often referred as the ray optics [6]. In order to determine the propagation of diffraction waves, the uniform geometrical theory of diffraction (UTD) is used.

In the conventional GO, the transport of energy between arbitrary two points in an isotropic lossless medium is accomplished using the conservation of the energy flux in a tube of rays. Within this tube of rays, the power of energy flux has to remain constant [6]:

$$S_0 dA_0 = S dA \quad (1)$$

where  $S_0$ ,  $S$  denote the radiation densities and  $dA_0$ ,  $dA$  are the cross-sectional areas of the tube at two different locations separated by a distance  $s$ . For TEM waves propagating in a medium characterized by the wave impedance  $Z_w$ ,  $S$  and the electric field intensity  $\mathbf{E}$  are related as follows [6]:

$$S = \frac{1}{2Z_w} |\mathbf{E}|^2 \quad (2)$$

Taking into account (1) and (2), we can write for an astigmatic tube of rays (Fig. 2) [6]:

$$\frac{|\mathbf{E}|}{|\mathbf{E}_0|} = \sqrt{\frac{dA_0}{dA}} = SAF = \sqrt{\frac{\rho_1 \rho_2}{(\rho_1 + s)(\rho_2 + s)}} \quad (3)$$

where  $SAF$  is a spreading attenuation factor,  $\rho_{1,2}$  are radii of curvature of the wave front at  $s=0$ . The right-hand side of (3) is called as a spreading attenuation factor in the literature.

The equation (3) relates the magnitude of the electric field at  $s$  to a reference magnitude at  $s=0$  only. In order to obtain an expression for the actual complex vector field, the Luneburg-Kline high-frequency expansion is adopted [6], and then

$$\mathbf{E}(s) = SAF e^{-j\beta s} \mathbf{E}_0 \quad (4)$$

where  $\mathbf{E}_0$  is the electric field intensity at the reference point ( $s=0$ ). If the transmitting antenna is modeled by a point source with a complex vector directional pattern  $\mathbf{C}_T$  and

gain  $G_T$  [9], the reference value of  $\mathbf{E}_0$  at the distance  $r_r$  from the antenna is given by [9]:

$$\mathbf{E}_0 = \sqrt{\frac{P_T G_T Z_w}{2\pi}} \frac{e^{-j\beta r_r}}{r_r} \mathbf{C}_T \quad (5)$$

where  $P_T$  denotes the input power of the transmitting antenna. The equation (5) is valid in the far field of the antenna only.

Apparently, the right-hand side of (3) becomes infinite for  $s = -\rho_1$  or  $s = -\rho_2$  (4), which means the approximation is no longer valid. The intersection of the rays at the lines 1-2 and 3-4 (Fig. 2) is called a caustic. When passing through a caustic in the direction of propagation, the sign of  $\rho + s$  changes and the correct phase shift of  $+\pi/2$  is introduced naturally. The equation (4) is a valid high-frequency approximation on both sides of the caustic, but the field near the caustic and at the caustic has to be found from separate considerations [7], [8]. Moreover, the equation (4) is valid if all the obstacles are large compared to the wavelength only.

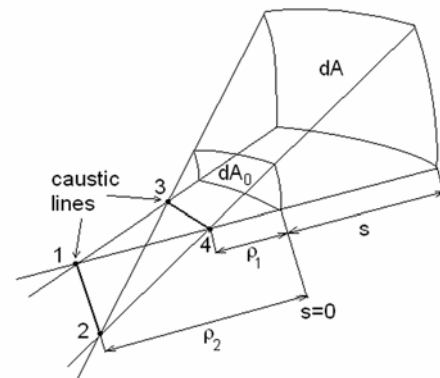


Fig. 2. Astigmatic tube of rays.

### 2.1 Propagation Phenomenon

In this part, the phenomena of the attenuation, reflection, transmission and diffraction of the electromagnetic wave are treated in a way enabling an easy usage in conjunction with the ray-optical approach discussed above.

#### 2.1.1 Absorption

If the electromagnetic wave propagates through the analyzed gases, the wave can be attenuated. The attenuation causes an exponential decay of the field intensity with the geometrical optics length [6]

$$\mathbf{E}(s) = e^{-\alpha s} \mathbf{E}_0 \quad (6)$$

where  $\alpha$  is the attenuation coefficient, which is defined as a real part of the complex propagation constant [6]

$$\gamma = \alpha + j\beta = j\omega\sqrt{\mu\varepsilon}\sqrt{1 + j\sigma/\omega\varepsilon}; \quad (7)$$

$\mu$ ,  $\varepsilon$  and  $\sigma$  are permeability, permittivity and conductivity.

### 2.1.2 Reflection and Refraction of Electromagnetic Wave

If a wave (a ray) impinges upon an interface, a reflected wave and a refracted one are formed according to Snell's law and the local plane wave approximation.

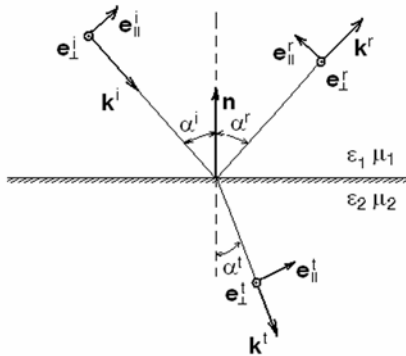


Fig. 3. Incident, reflected and refracted wave.

For evaluation, the incident wave is decomposed into two orthogonal polarizations (parallel one and perpendicular one) which are treated separately (Fig. 3). Then, the total field is given by the vector sum of two components.

If the incident wave  $\mathbf{E}^i$  (ray) impinges upon a planar interface, the reflected wave  $\mathbf{E}^r$  at  $Q$  is described by [6]

$$\mathbf{E}^r(Q) = \mathbf{R} \mathbf{E}^i(Q). \quad (8)$$

Similarly, the refracted wave  $\mathbf{E}^t$  at the  $Q$  is described by [6]

$$\mathbf{E}^t(Q) = \mathbf{T} \mathbf{E}^i(Q). \quad (9)$$

The dyadic reflection coefficient  $\mathbf{R}$  and the dyadic transmission coefficient  $\mathbf{T}$  are given by [6]

$$\mathbf{R} = R_{\parallel} \mathbf{e}_{\parallel}^r \mathbf{e}_{\parallel}^i + R_{\perp} \mathbf{e}_{\perp}^r \mathbf{e}_{\perp}^i, \quad (10)$$

$$\mathbf{T} = T_{\parallel} \mathbf{e}_{\parallel}^t \mathbf{e}_{\parallel}^i + T_{\perp} \mathbf{e}_{\perp}^t \mathbf{e}_{\perp}^i, \quad (11)$$

with

$$\mathbf{e}_{\perp}^t = \mathbf{e}_{\perp}^r = \mathbf{e}_{\perp}^i = \frac{\mathbf{n} \times \mathbf{k}^i}{|\mathbf{n} \times \mathbf{k}^i|}, \quad (12)$$

$$\mathbf{e}_{\parallel}^i = \mathbf{k}^i \times \mathbf{e}_{\perp}^i, \mathbf{e}_{\parallel}^r = \mathbf{k}^r \times \mathbf{e}_{\perp}^r, \mathbf{e}_{\parallel}^t = \mathbf{k}^t \times \mathbf{e}_{\perp}^t, \quad (13a,b,c)$$

where  $R_{\parallel}$ ,  $R_{\perp}$  and  $T_{\parallel}$ ,  $T_{\perp}$  are Fresnel's reflection and transmission coefficients for parallel and perpendicular polarization [6]. Symbols  $(\mathbf{k}^i, \mathbf{e}_{\perp}^i, \mathbf{e}_{\parallel}^i)$ ,  $(\mathbf{k}^r, \mathbf{e}_{\perp}^r, \mathbf{e}_{\parallel}^r)$  and  $(\mathbf{k}^t, \mathbf{e}_{\perp}^t, \mathbf{e}_{\parallel}^t)$  are orthonormal bases generated by the direction of the incidence  $\mathbf{k}^i$ , the direction of the reflection  $\mathbf{k}^r$  and the direction of the refraction  $\mathbf{k}^t$  (Fig. 3), respectively.

The above formulas are valid only for a uniform plane wave impinging on an infinite smooth planar boundary. However, these formulas can be used even if dimensions of the interface are finite, but large compared to wavelength.

If the interface is curved, the reflection and the transmission can be still treated by ray-optical methods if the radii of curvature of the surface are large enough. If this condition is fulfilled, the reflected wave  $\mathbf{E}^r$  at a distance  $s$  from the reflection point  $Q$  can be described by [6]

$$\mathbf{E}^r(Q) = SAF^r \exp(-j\beta s) \mathbf{R} \mathbf{E}^i(Q) \quad (14)$$

with

$$SAF^r = \sqrt{\frac{\rho_1^r \rho_2^r}{(\rho_1^r + s)(\rho_2^r + s)}}. \quad (15)$$

Similarly, the refracted wave  $\mathbf{E}^t$  at a distance  $s$  from the point of refraction  $Q$  is given by

$$\mathbf{E}^t(Q) = SAF^t \exp(-j\beta s) \mathbf{T} \mathbf{E}^i(Q) \quad (16)$$

with

$$SAF^t = \sqrt{\frac{\rho_1^t \rho_2^t}{(\rho_1^t + s)(\rho_2^t + s)}}. \quad (17)$$

In (15) and (17),  $\rho_1^r$ ,  $\rho_2^r$  and  $\rho_1^t$ ,  $\rho_2^t$  are principal radii of curvature of the reflected wave and the refracted one [9]. These radii depend on the principal radii of curvature of the incident wave and the interface.

### 2.1.3 Diffraction of Electromagnetic Wave

If a wave impinges upon an edge, the uniform theory of diffraction can be applied to calculate the diffracted field. According to that theory, the possible diffracted rays leave the edge in a cone of an internal half-angle lying on the far side of the plane normal to the edge (Fig. 4) [6], [10], [11]. The diffracted field can be described by [6], [10]

$$\mathbf{E}^d(Q_d) = SAF^d \exp(-j\beta s) \mathbf{D} \mathbf{E}^i(Q_d), \quad (18)$$

where  $SAF^d$  is a spreading attenuation factor of the diffracted field [6],  $s'$  is the path length from the transmitter  $T_x$  to the diffraction point  $Q_d$ , and  $s$  is the path length from the diffraction point  $Q_d$  to the receiver  $R_x$ . The dyadic edge diffraction coefficient  $\mathbf{D}$  is given by [6]

$$\mathbf{D} = D_s \boldsymbol{\beta}'_0 \boldsymbol{\beta}_0 + D_h \boldsymbol{\varphi}'_0 \boldsymbol{\varphi}_0, \quad (19)$$

with

$$\boldsymbol{\varphi}' = \frac{\mathbf{s}' \times \mathbf{t}}{|\mathbf{s}' \times \mathbf{t}|}, \quad \boldsymbol{\varphi} = \frac{\mathbf{s} \times \mathbf{t}}{|\mathbf{s} \times \mathbf{t}|}, \quad (20a, b)$$

$$\boldsymbol{\beta}'_0 = \mathbf{s}' \times \boldsymbol{\varphi}', \quad \boldsymbol{\beta}_0 = \mathbf{s} \times \boldsymbol{\varphi}. \quad (21a, b)$$

In (19),  $D_s$  and  $D_h$  are the diffraction coefficients for the soft polarization and the hard polarization<sup>1</sup> [6]. Symbols  $(\mathbf{s}', \boldsymbol{\varphi}', \boldsymbol{\beta}')$  and  $(\mathbf{s}, \boldsymbol{\varphi}, \boldsymbol{\beta})$  denote orthonormal bases

<sup>1</sup> The terms *soft polarization* and *hard polarization* are not generally known. They should be therefore briefly explained here.

generated by the direction of the incidence  $s'$  and the direction of the diffraction  $s$  (Fig. 4), respectively. Finally, the vector  $t$  is tangential vector to the edge at a point  $Q_d$ .

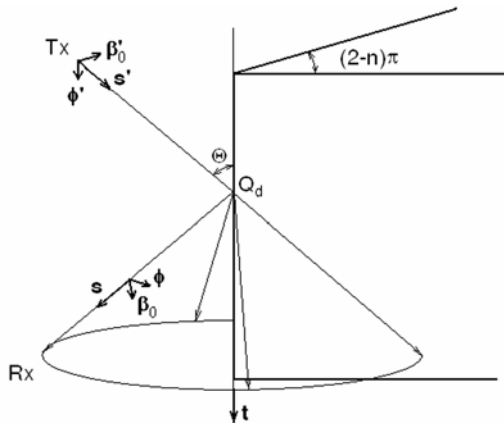


Fig. 4. Diffraction by an edge.

If a ray hits the edge, the edge becomes secondary source. All the rays radiating from the edge are traced as a usual ray. Since the strength of the diffracted ray is weak, the 2<sup>nd</sup> order diffraction and the higher-order one are neglected.

The phrase “a ray hits the edge” draws that a ray hits a certain surface in the vicinity of the edge defined by the maximum distance  $d_{max}$  (Fig. 5) at a point  $Q_d$ . In order to avoid phase errors, this distance should be as small as possible, but the number of rays should be sufficient enough to provide good scanning of the wedge. The maximum distance  $d_{max}$  should be therefore chosen about  $\lambda/15$  as a compromise of these claims. The diffracted rays start at a point  $Q'_d$  which is a projection of the point  $Q_d$  on the edge.

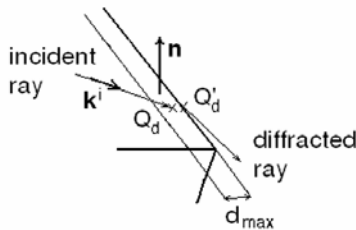


Fig. 5. Vicinity of an edge.

## 2.2 Field Intensity Calculation

If a propagation path of a ray was found with  $m$  reflections,  $o$  refractions and  $p$  diffractions (according to the above section,  $p$  can be 0 or 1), then the field intensity of a single ray at the receiver can be evaluated by [11]

$$E_R = E_0 \cdot \prod_{a=1}^m SAF_a^r \mathbf{R}_a \exp(-\gamma_a s_a) \cdot \prod_{b=1}^o SAF_b^t \mathbf{T}_b \exp(-\gamma_b s_b) \cdot \prod_{c=1}^p SAF_c^d \mathbf{D}_c \exp(-\gamma_c s_c). \quad (22)$$

However, if ray-launching is applied, a large number of rays  $l$  reach the receiver on different propagation paths. Thus, the resulting field at the receiver is given by the vector sum of all the rays (22)

$$E_{R,tot} = \sum_{e=1}^l E_{R,e}. \quad (23)$$

## 3. Ray Density Normalization and Calculation of the Field

As discussed in the introduction, if the ray-launching with the reception spheres is applied, the determination of the diameters of spheres is difficult because important propagation paths may not be considered or several physically identical rays might be reached by the receiver. In order to overcome this trouble, the ray density normalization can be used [5].

Each physical path is a priori presented by several multiple rays in this approach. The number of these rays is determined, and is used to normalize the contribution of each ray to the total field. The precondition of the ray density normalization is that a large number of rays from the transmitter have to be distributed homogeneously.

### 3.1 Determining the Number of Multiple Rays

For  $N$  discrete rays launched from the transmitter assuming a plane surface, the ray density at a distance  $r$  (an unfolded path length) is given by [5]

$$n_d = \frac{N}{4\pi r^2}. \quad (24)$$

If reflections or refractions at curved boundary occur, the proportionality  $1/r^2$  is not valid longer, because the rays can be focused or defocused. For the ray density at a distance  $s$  from the curved surface, the ray density after the reflection is given by [5]

$$n_d^r(s) = \left| \frac{\rho_1^r \rho_2^r}{(\rho_1^r + s)(\rho_2^r + s)} \right| n_d^i. \quad (25)$$

Similarly, the ray density after the refraction can be expressed as

$$n_d^t(s) = \left| \frac{\rho_1^t \rho_2^t}{(\rho_1^t + s)(\rho_2^t + s)} \right| n_d^i \quad (26)$$

where  $n_d^i$  denotes the incident ray density at a surface,  $n_d^r$  and  $n_d^t$  are the ray density after reflection and refraction at the distance  $s$  from the point of reflection and refraction, respectively. Next,  $\rho_1^r, \rho_2^r$  and  $\rho_1^t, \rho_2^t$  are the principal radii of curvature [9] of the reflected and refracted wave after reflection and refraction, respectively. The ray density before the first reflection or refraction is given by (24).

The total number of rays  $M$  reaching the receiver by the same propagation path is

$$M = n_d A \quad (27)$$

where  $A$  is a “visible” area of a receiver.

The above calculation of the number of rays reaching the receiver at the same propagation path was described in [5]. This calculation is valid only if rays are not obstructed, reflected or refracted. This calculation is not valid for the diffraction. Thus, we extend the theory of the ray density for diffracted rays.

If the diffraction occurs, we have to take into account the original ray density, computed according to the relations (24) to (26), and further, we have also to take into account the fact that the incident wave excites diffracted rays. Let us denote the number of rays, which are launched from the point of diffraction  $Q'_d$  in a cone (Fig. 4, 5), by the symbol  $N^d$ .

The original ray density computed according to the relations (24) to (26) has to be modified, because only those incident rays are considered which impinge on the edge and its vicinity defined by the distance  $d_{\max}$ , and the diffracted rays are launched from the edge. Let's call it as the ray density parallel to the edge and denote it  $n_d^{\text{par}}$ . Taking the above facts into account, and considering the influence of the diffraction edge on the incident wave [6], principal radii of the wavefront, and assuming the plane surface, we obtain the following relation for the ray density parallel to the edge at a distance  $r$  (unfolded path length) from the point  $Q'_d$

$$n_d^{\text{par}} = \frac{\rho_c}{(\rho_c + r)} n_d^i d_{\max} |\mathbf{n} \cdot \mathbf{k}^i| \quad (28)$$

where  $n_d^i$  denotes the incident ray density (24) to (26),  $\rho_c$  is a radius of curvature of the diffracted wave in the diffraction plane,  $\mathbf{n}$  is a normal to the wedge, and  $\mathbf{k}^i$  is a propagation direction of the incident wave (Fig. 5).

Obviously, an incident ray excites  $N^d$  diffracted rays which leave an edge in a cone. The ray density of these rays, let's call it as the ray density perpendicular to the edge and denote it  $n_d^{\text{dper}}$ , depends on the number of diffracted rays, the angle of the wedge  $2n\pi$  and the angle of the incident ray  $\Theta$ . Taking the above facts into account and assuming the plane surface, we obtain the following relation for the ray density perpendicular to the edge at a distance  $r$  (unfolded path length) from the point  $Q'_d$

$$n_d^{\text{dper}} = \frac{N^d}{2n\pi r \sin \Theta}. \quad (29)$$

The total ray density after the diffraction is evaluated as the product of both the ray densities (28) and (29)

$$n_d^d = n_d^{\text{par}} n_d^{\text{dper}}. \quad (30)$$

If reflections or refractions at curved boundary occur, the equations (25) and (26) can be used with (30).

The total number of rays  $M^d$  (the rays started at the point of diffraction) reaching the receiver at the same propagation path is

$$M^d = n_d^d A \quad (31)$$

where  $A$  is a “visible” area of a receiver.

To be noticed, the number of rays  $M$  or  $M^d$  is an integer and finite number.

## 3.2 Field Calculation

For the field calculation using ray density, two approaches can be used: the field trace and the power trace [5]. In this part, we introduce a power-field trace, which stands on the idea of a power trace; however, it is more general than the power trace [5].

### 3.2.1 Field Trace

The field trace is a conventional approach in ray-launching. A certain electric field is assigned to each ray, and rays are traced until they hit a receiver, or until their attenuation does not reach a desired level.

If the ray density normalization is used, each single ray has to be normalized by the number of rays  $M$  which travel along the same physical path. The electric field intensity of a single ray can be computed if the diffraction does not occur

$$\mathbf{E}_R = \frac{1}{M} \prod_{a=1}^m SAF_a^r \mathbf{R}_a \exp(-\gamma_a s_a) \cdot \prod_{b=1}^o SAF_b^t \mathbf{T}_b \exp(-\gamma_b s_b) \cdot \mathbf{E}_0. \quad (32a)$$

If the diffraction occurs

$$\mathbf{E}_R = \frac{1}{M^d} \prod_{a=1}^m SAF_a^r \mathbf{R}_a \exp(-\gamma_a s_a) \cdot \prod_{b=1}^o SAF_b^t \mathbf{T}_b \exp(-\gamma_b s_b) \cdot \prod_{c=1}^p SAF_c^d \mathbf{D}_c \exp(-\gamma_c s_c) \cdot \mathbf{E}_0. \quad (32b)$$

The resulting field at the receiver is given by the vector sum of all the rays (32). The meaning of the symbols  $m$ ,  $o$ ,  $p$  is the same as in (22).

### 3.2.2 Power Trace

The basic idea of the power trace assumes that the total power radiated by the transmitting antenna is spread over all the rays, each ray keeps its portion of the power of wave, and attenuation may occur due to the propagation phenomena [5]. If a ray hits a receiver, its remaining power is transferred to the receiver. The effect of the free-space attenuation is included implicitly. Increasing the distance,

the number of rays, and consequently the smaller power reaches the receiver.

The power trace in combination with the ray density normalization [5] allows to overcome one of the major disadvantages of GO and the field trace – their failure at caustics, where the predicted field approaches infinity [6]. However, the original approach is a bit ponderous for our application because the electric field distribution is the quantity of interest, and further, the original approach does not take the diffraction into account. Thus, we derive the approach called power-field trace, which stands on the idea of power trace, however, is more general and takes the diffraction into the account.

### 3.2.3 Power-Field Trace

The initial power of each ray is given by

$$P_i = P_T G_T |C_T|^2 / N \quad (33)$$

where  $N$  is the number of launched rays. If a ray hits a receiver with the aperture  $A$ , the ray is assumed to deliver its total energy (if no propagation loss occurs) to the receiver. Then, the following radiation density (the power of a ray spreads over a receiver aperture) is produced:

$$S_A = P_i / A. \quad (34)$$

The approximation is valid only for

$$A_{rt} \leq A, \quad (35)$$

where  $A_{rt}$  is the actual area of the ray tube.

Since assembling all the rays, which reach the receiver, makes sense in physical terms for power trace only, let us sum up rays traveling along the same physical path. According to the equations (24) to (31), we have to sum up  $M$ , or  $M^d$  rays. Then, the total power density at the receiver is

$$S = \sum_{k=1}^M S_{A,k} = \sum_{k=1}^M \frac{P_{t,k}}{A} = \frac{P_t}{A} M. \quad (36)$$

By substituting (33) and (36) into (2), we get

$$|E|^2 = 2Z_w P_T G_T \frac{M}{NA} |C_T|^2. \quad (37)$$

Since complex directivity pattern  $C_T$  of the transmitting is of the same orientation as the intensity of the electric field (5), and the wavefront changes its phase along the propagation path, we can write

$$E = \sqrt{2Z_w P_T G_T \frac{M}{NA}} \exp(-j\beta r) C_T. \quad (38)$$

The equation (38) can be used for the evaluation of the electric field of the transmitting antenna, which is modeled by a point source with the complex vector directional pattern  $C_T$  and gain  $G_T$ , at the distance  $r$ .

For the verification of the above considerations, let us assume that  $N$  rays are homogeneously distributed between the transmitter and at distance  $r$  from the transmitter. The

ray density can be computed according to (24). After that, the receiver aperture  $A$  at distance  $r$  is reached by  $M$  rays

$$M = \frac{AN}{4\pi r^2}. \quad (39)$$

By substituting (39) to (38), we get

$$E = \sqrt{\frac{Z_w P_T G_T}{2\pi} \frac{\exp(-j\beta r)}{r}} C_T \quad (40)$$

which equals to (5) for  $r = r_r$ . Thus, eqn. (38) is valid.

The fraction  $[M/(NA)]^{1/2}$  in (38) stands for a spatial divergence factor  $SAF$  along the whole propagation path of a ray. In order to include reflection, refraction and diffraction phenomena, dyadic coefficients have to be added similarly as described in Section 2.

Before formulating the field intensity of a single ray, the numerator and the denominator of (38) is multiplied by  $2\pi^{1/2}r$  and  $r=r_r$ , and the formula (38) can be rewritten

$$\begin{aligned} E &= \sqrt{2Z_w P_T G_T \frac{M}{NA}} \exp(-j\beta r) C_T \frac{2\sqrt{\pi}r}{2\sqrt{\pi}r} \\ &= \sqrt{\frac{M}{AN} 4\pi r^2} E_0. \end{aligned} \quad (41)$$

Taking into account the normalization by  $M$  rays, the dyadic coefficients  $\mathbf{R}$ ,  $\mathbf{T}$ ,  $\mathbf{D}$  and the spreading divergence factor  $SAF$ , the field intensity of a single ray can be represented by the fraction  $[M/(NA)]^{1/2}$  for the whole propagation path, and can be evaluated according to the following relation if the diffraction does not occur

$$\begin{aligned} E_R &= \frac{1}{M} \prod_{a=1}^m \mathbf{R}_a \exp(-\gamma_a s_a) \cdot \\ &\quad \cdot \prod_{b=1}^o \mathbf{T}_b \exp(-\gamma_b s_b) \cdot \sqrt{\frac{M 4\pi r^2}{NA}} E_0 \\ &= \sqrt{\frac{4\pi r^2}{MNA}} \prod_{a=1}^m \mathbf{R}_a \exp(-\gamma_a s_a) \cdot \\ &\quad \cdot \prod_{b=1}^o \mathbf{T}_b \exp(-\gamma_b s_b) \cdot E_0, \end{aligned} \quad (42a)$$

and if the diffraction occurs

$$\begin{aligned} E_R &= \frac{1}{M^d} \prod_{a=1}^m \mathbf{R}_a \exp(-\gamma_a s_a) \cdot \\ &\quad \cdot \prod_{b=1}^o \mathbf{T}_b \exp(-\gamma_b s_b) \cdot \\ &\quad \cdot \prod_{c=1}^p \mathbf{D}_c \exp(-\gamma_c s_c) \cdot \sqrt{\frac{M^d 4\pi r^2}{NA}} E_0 \\ &= \sqrt{\frac{4\pi r^2}{M^d NA}} \prod_{a=1}^m \mathbf{R}_a \exp(-\gamma_a s_a) \cdot \\ &\quad \cdot \prod_{b=1}^o \mathbf{T}_b \exp(-\gamma_b s_b) \cdot \\ &\quad \cdot \prod_{c=1}^p \mathbf{D}_c \exp(-\gamma_c s_c) \cdot E_0. \end{aligned} \quad (42b)$$

Obviously, equations (42) are analogous to equations (32).

The resulting field at the receiver is given by the vector sum of all rays

$$\mathbf{E}_{R,tot} = \sum_{e=1}^l \mathbf{E}_{R,e}. \quad (43)$$

The described approach does not fail at caustics, because the number of rays  $M$  or  $M^d$  is finite, and their maximum equals to the number of transmitted rays or their fraction. This is the most important advantage compared to the approach described in Section 3.2.1.

## 4. Modeling Spectrometer

So that the above-discussed ray-launching approach can become an efficient tool for modeling the spectrometer, an intersection of a ray and an object (e.g., a spectrometer component) must be computed precisely analytically.

Since the distribution of the electromagnetic field in a plane is required to be known, standalone reception spheres cannot be used, because a large number of spheres are needed. Thus, a reception plane or block is used.

The „reception plane” is a part of a plane which is divided into small reception elements (rectangles). In order to decide whether an element of the reception plane was hit by a ray, an intersection of a ray with the plane is computed only. In case of reception spheres, a large number of intersections with reception spheres have to be checked (computed). However, the reception plane fails if most rays are parallel to it. In such a case, a reception plane has to be appropriately packed by a block, and a reception block has to be used. Then, we have to compute whether at least one of brick’s walls is hit by a ray. If this is true, the ray is projected into the reception plane of the reception block, and the intersections of the projected ray with the elements of the reception plane are computed. Exploitation of the reception block is more time-consuming than the usage of the reception plane. On the other hand, the described approach is more general than the reception plane, and is less time consuming compared to the reception spheres.

### 4.1 Analyzing Lens

The proposed approach is verified by the analysis of a lens (a component of the spectrometer) which is excited by a half-wavelength dipole placed at the focus of the lens. The operation frequency is 60 GHz (Fig. 6). The focal length of the lens is 200 mm, and its diameter is 200 mm. The structure is analyzed by CST Microwave Studio and by the proposed ray-launching approach. For the ray launching method, dipole is modeled by its directivity pattern.

Results obtained both by the CST Microwave Studio and the ray-launching are depicted in Fig. 7. The distribution of the electric field intensity along the axis of the lens (the blue line in Fig. 6) depends on the distance from the

dipole. The comparison of results shows that the accuracy of the proposed approach is very good.

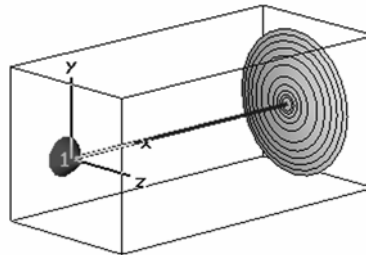


Fig. 6. Analyzed lens excited by a half-wavelength dipole.

### 4.2 Analyzing Spectrometer

The analyzed part of the spectrometer is depicted in Fig. 8. The distribution of the electrical field intensity is computed in the box bounded by the dashed lines only. The length of the box is  $L = 2.6$  m and the width is  $W = 0.55$  m.

The spectrometer is analyzed at  $f = 118.75$  GHz. The cell is of a cylindrical shape, and is made from glass. The length of the cell is 2.0 m, the diameter is 0.1 m, and the thickness of the wall of the sample cell is 0.005 m.

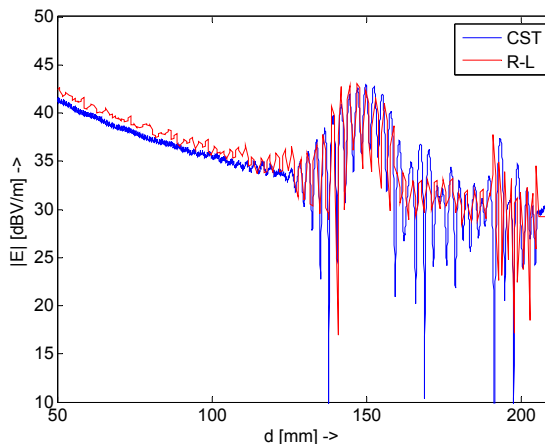


Fig. 7. Dependence of electric field intensity on the distance from the dipole. The lens is situated at  $d = 200$  mm. Field intensity was computed by CST (blue line) and by ray-launching (red line).

Horn antennas are used in the spectrometer. The gain of the transmitting antenna is  $G = 20$  dB and its directivity pattern is used during the analysis. The antenna is fed by the power 10 mW. The focal length of used lenses is 0.2 m and their diameter is 0.1 m. The lenses (hyperbolic surfaces) are made from Teflon with the relative permittivity 2.08.

For the analysis, 8 640 000 rays are launched from the transmitting antenna.

The result of the spectrometer analysis by the ray-launching method, i.e. the distribution of the electric field intensity in the cell, is depicted in Fig. 9. The enlarged details of the field distribution in the vicinity of selected components of the spectrometer are depicted in Figs 10 to 15. Fig. 9 illustrates the way how the radiated energy

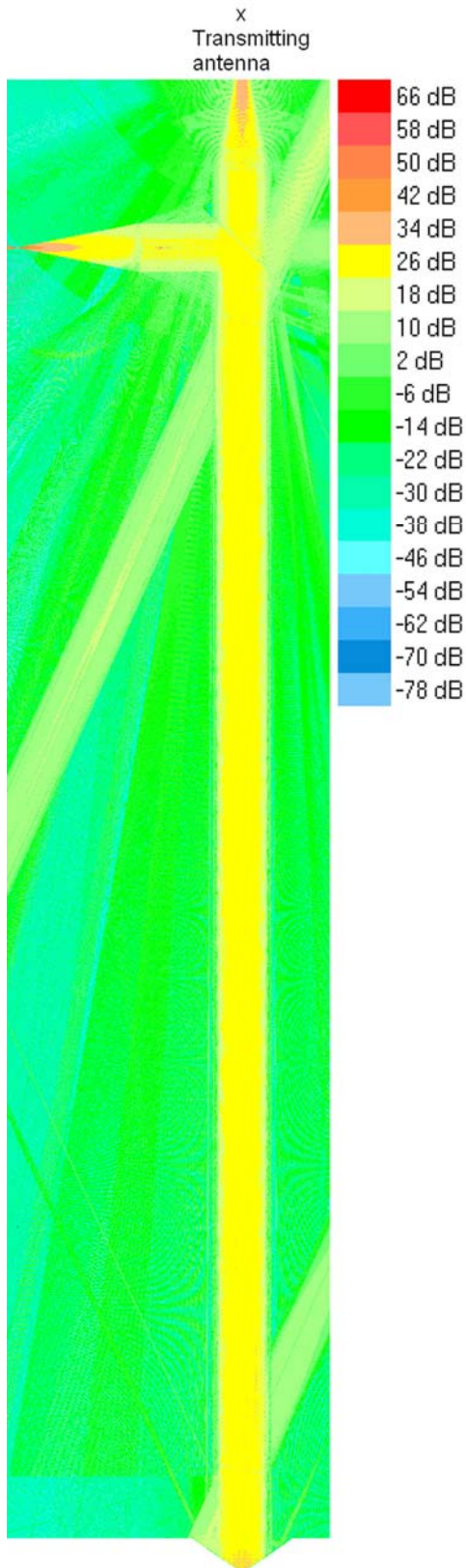


Fig. 9. Distribution of the electric field intensity of the spectrometer.

travels from the transmitting antenna through the spectrometer, is focused and defocused.

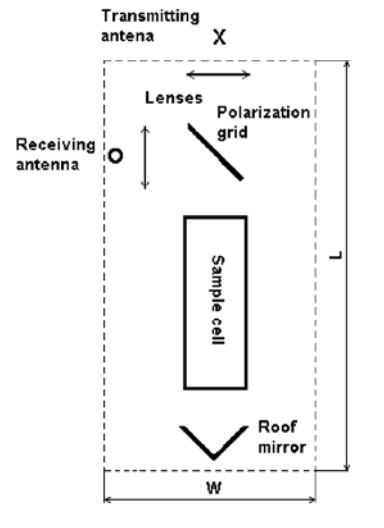


Fig. 8. Analyzed spectrometer.

The distribution of the electric field intensity in the vicinity of the lens of the transmitting antenna is depicted in Fig. 10. The distribution of the intensity of the electric field along the black line, drawn in this picture, is depicted in Fig. 11. Obviously, a caustic point of the lens can be identified here, the standing wave ratio (SWR) in front of the lens is about 5 dB, and is negligible behind the lens.

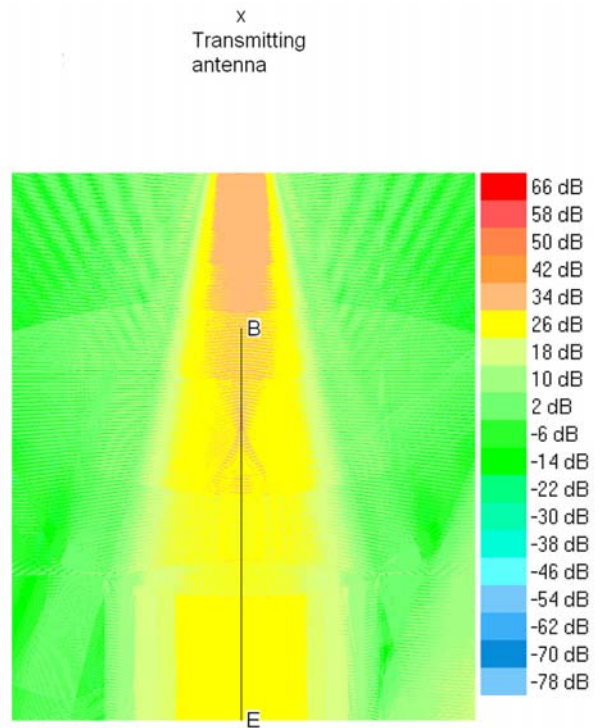


Fig. 10. Distribution of the electric field intensity in the vicinity of the lens at the transmitting antenna.

Whereas the space between the transmitting antenna and the lens is in the near field region of the antenna, the lens and the space behind the antenna is in the far field region of the transmitting antenna. Thus, the evaluated field in front of the antenna is corrupted by an error, and the results in this region have to be considered as illustrative ones

only. However, the rest of results is “valid” according to the theory mentioned above.

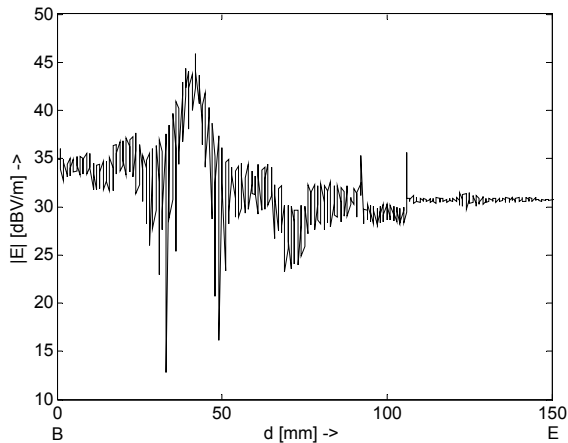


Fig. 11. Distribution of the electric field intensity along the black line drawn in Fig. 10.

The distribution of the electric field intensity in the vicinity of the lens of receiving antenna is depicted in Fig. 12. The distribution of the electric field intensity along the black line, drawn in this picture, is depicted in Fig. 13. Obviously, the energy is focused to the focal point of the lens. SWR is almost negligible in front of the lens (seen from the sample cell), and reaches about 5 dB in the lens.

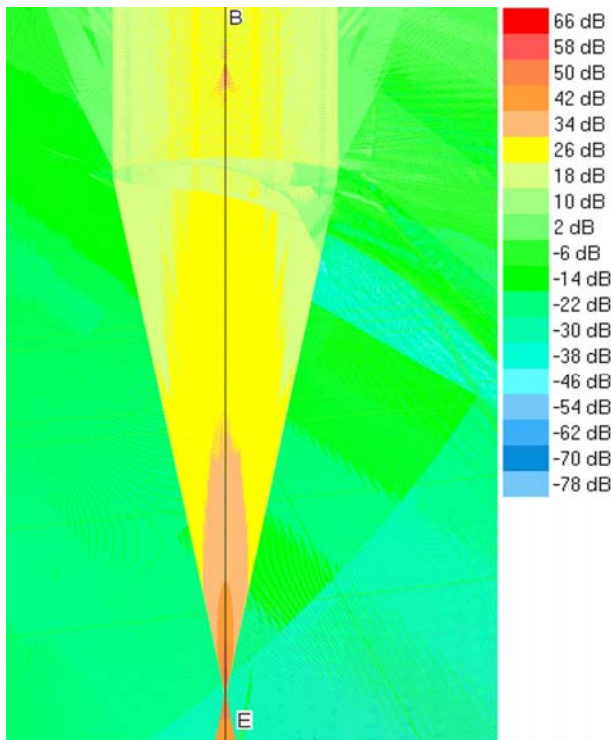


Fig. 12. Distribution of the electric field intensity in the vicinity of the lens at the receiving antenna (the figure is rotated).

The distribution of electric field intensity in the vicinity of the reflector and at the reflector in the end of the sample cell is depicted in Fig. 14. The distribution of the intensity of the electric field along the black line, drawn in this picture, is depicted in Fig. 15. Obviously, a large fluctuation of the field (nearly 10 dB) appears near the reflector. SWR in sample cell is up to 3 dB.

tuation of the field (nearly 10 dB) appears near the reflector. SWR in sample cell is up to 3 dB.

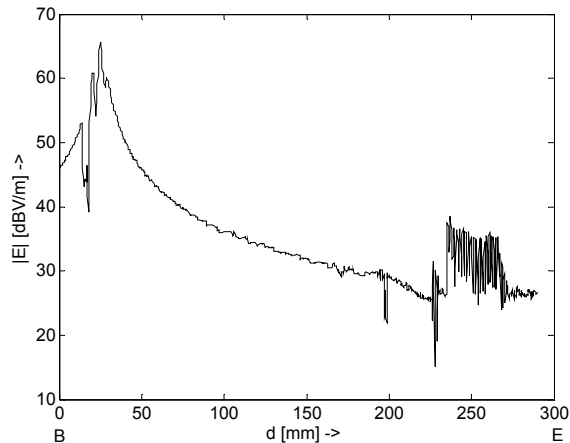


Fig. 13. Distribution of the electric field intensity along the black line drawn in Fig. 12.

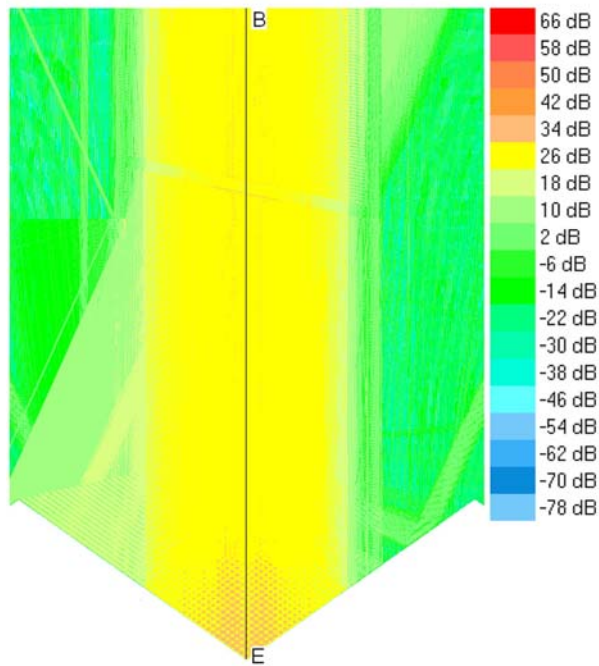


Fig. 14. Distribution of the electric field intensity in the vicinity of the reflector.

### 5. Conclusion

In this paper, the ray launching method with the ray density approach was extended to take the diffraction into account, and the power-field trace was proposed. The accuracy of the presented approach was verified by the analysis of a spectrometer component – a lens. The lens was analyzed in CST Microwave Studio first, and then, the analysis was repeated by the developed ray-launching method. Comparisons prove good accuracy of presented approach.

The developed method was used for modeling a rotational spectrometer in order to obtain the distribution of the

electric field intensity. The results from this analysis can be used for the optimization of the spectrometer.

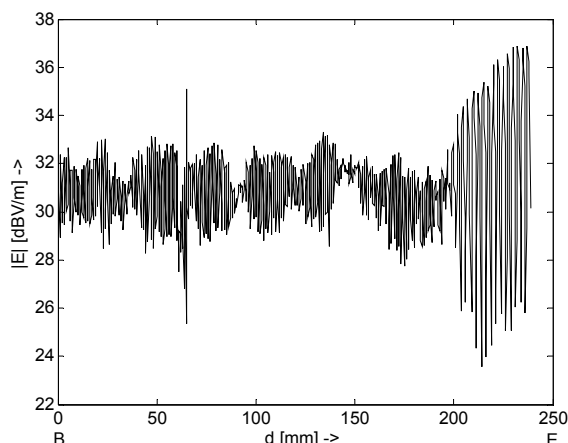


Fig. 15. Distribution of the electric field intensity along the black line drawn in Fig. 14.

## Acknowledgements

The presented research was financially supported by the Centre for Quasioptical Systems and Terahertz Spectroscopy LC06071. The research is the part of the COST Action IC 0603 "Antenna Systems & Sensors for Information Society Technologies (ASSIST)".

## References

- [1] KANIA, P. *Rotational-Hyperfine Spectroscopy of Important Atmospheric Molecules*. Ph.D. Thesis, VSCHT Prague 2006. (In Czech)

- [2] CHEW, W., C., JIN, J., M., MICHIELSEN, E., SONG, J., M. *Fast and Efficient Algorithms in Computational Electromagnetics*, Boston, MA: Artech House, 2001.
- [3] YANG, C. F., WU, B., C., KO, C. J. A ray-tracing method for modeling indoor wave propagation and penetration. *IEEE Trans. on Antennas and Propagation*, 1998, vol. 46, no. 6, p. 907-919.
- [4] SEIDL, S. Y., RAPPAPORT, T. S. Site-specific propagation prediction for wireless in-building personal communication system design. *IEEE Transactions on Vehicular Technology*, 1994, vol. 43, no. 4, p. 879-891.
- [5] DIDASCALOU, D., SCHAFFER, T. M., WEINMANN, F., WIESBECK, W. Ray-density normalization for ray-optical wave propagation modeling in arbitrarily shaped tunnels. *IEEE Trans. on Antennas and Propagation*, 2000, vol. 48, no. 9, p. 1316-1325.
- [6] BALANIS, C. A., *Advanced Engineering Electromagnetics*. John Wiley&Sons, 1989.
- [7] KOUYOUMJIAN, R. G. Asymptotic high frequency methods. *Proc. IEEE*, 1965, vol. 53, pp. 864-876.
- [8] KAY, I., KELLER, J. B. Asymptotic evaluation of the field at a caustic. *J. Appl. Phys.*, 1954, vol. 25, pp. 876-883.
- [9] LEE, S. W. Reflection at a curved dielectric interface: Geometrical optics solution. *IEEE Transactions on Microwave Theory and Techniques*, 1982, vol. 30, no. 1, p. 12-19.
- [10] LUEBBERS, R. J. Finite conductivity uniform GTD versus knife edge diffraction in prediction of propagation path loss. *IEEE Transactions on Antennas and Propagation*, 1984, vol. 32, no. 1, p. 70-76.
- [11] BARCLAY, L. *Propagation of Radiowaves*. 2nd Edition, IEE, United Kingdom, 2003.
- [12] www.cst.com

## About Authors...

Jaroslav LÁČÍK, Zbyněk LUKEŠ, and Zbyněk RAIDA – for biographies, see page 95 of the December 2006 issue of the journal.

# RADIOENGINEERING REVIEWERS

June 2008, Volume 17, Number 2

- ČERNOCKÝ, J., Brno University of Technology
- DRUTAROVSKÝ, M., Technical University of Košice, Slovakia
- FISCHER, J., Czech Technical University in Prague
- FRÝZA, T., Brno University of Technology
- GRGIC, M., University of Zagreb, Croatia
- HALÁMEK, J., Academy of Sciences of the Czech Republic, Brno
- HARTÁNSKÝ, R., University of Trenčín, Slovakia
- HOZMAN, J., Czech Technical University in Prague
- KOLKA, Z., Brno University of Technology
- KRATOCHVÍL, T., Brno University of Technology
- KRŠEK, P., Brno University of Technology
- MOHR, F., University of Applied Sciences Pforzheim
- MÜLLER, L., University of West Bohemia in Pilsen
- NOUZA, J., Technical University of Liberec
- PETRŽELA, J., Brno University of Technology
- PIKSA, P., Czech Technical University in Prague
- PROVAZNÍK, I., Brno University of Technology
- RAIDA, Z., Brno University of Technology
- RAVAS, R., Slovak University of Technology, Bratislava, Slovakia
- SOVKA, P., Czech Technical University in Prague
- SVAČINA, J., Brno University of Technology
- ŠIMŠA, J., Academy of Sciences of the Czech Republic, Prague
- TRÚCHLY, P., Slovak University of Technology, Bratislava, Slovakia